Target Tracking with Variational Multi-Detection Mode under Unknown Parameters for HFHSSWR

Longyuan XU [1,2], Peng TONG [1,2], Yinsheng WEI [1,2]

[1]Dept. of Electronic Engineering, Harbin Institute of Technology, 150001 Harbin, China
[2]Dept. of Key Laboratory of Marine Environmental Monitoring and Information Processing, Ministry of Industry and Information Technology, 150001, Harbin, China

22b905019@stu.hit.edu.cn, tongpeng@hit.edu.cn, hitweiysgroup@163.com

Submitted March 1, 2024 / Accepted May 31, 2024 / Online first June 17, 2024

Abstract. *The shipborne High-Frequency Hybrid Sky-Surface Wave Radar integrates a sky-wave transmitting channel and a ground-wave receiving channel on a shipborne platform. This hybrid radar system combines a skywave source with the added flexibility of a far-away shipborne radar. Ionospheric stratification and height uncertainty introduce uncertainties in the sky-wave channel, resulting in multiple measurements of one target. Additionally, the shipborne platform position is affected by sea state, causing errors in azimuth accuracy setting and subsequently reducing target tracking precision. In this paper, we propose for the first time a target tracking method that combines ionospheric variations with the motion of a shipborne platform. It introduces the variational Bayesian method into the multiple detection mode, which solves the effects of ionospheric altitude error and orientation error of shipborne platforms due to different sea states on target tracking. Simulation experiments validate the effectiveness of the proposed method. Therefore, the proposed method promises advancements in shipborne radar systems for maritime surveillance applications.*

Keywords

Shipborne HFHSSWR, target tracking methods, ionospheric disturbance, unknown parameters

1. Introduction

The shipborne High-Frequency Hybrid Sky-Surface Wave Radar (HFHSSWR) represents a novel hybrid propagation mode over-the-horizon radar, combines the capabilities of sky-wave High-Frequency (HF) radar with shipborne surface-wave HF radar [1], [2]. In this configuration, the transmitting station, situated inland, emits electromagnetic waves that are reflected to the target through the ionosphere. The waves scattered by the target are then captured by the shipborne receiving station via radiation of surface wave. While HFHSSWR offers the expansive coverage of sky-wave HF radar and the flexibility of shipborne surface-wave HF radar, the intersection of these two systems introduces new challenges not only in signal processing but also in target tracking. Current research on shipborne HFHSSWR mainly focuses on the effects of the ionosphere and shipborne platforms on sea clutter, as well as effective suppression methods [3], [4]. However, there is relatively limited research in the area of target tracking. In summary, the issues can be outlined as follows:

1) Due to the limited size of the antenna array on the shipborne platform, azimuth measurement errors frequently surpass 2° in magnitude [5]. Accurately quantifying this error proves challenging due to variations in sea clutter caused by fluctuating sea states. Moreover, the movement of the shipborne platform significantly broadens the sea clutter, diminishing the likelihood of detecting slow-moving targets like ships [6]. This leads to low measurement accuracy, variable measurement error and low detection probability for radars in this regime;

2) The radar encounters diverse propagation modes in signal echoes due to ionospheric stratification characteristics. The unstable ionosphere further exacerbates this complexity, leading to a phenomenon where the accuracy of target tracking is significantly reduced.

Therefore, it is imperative to investigate a target tracking method tailored to the shipborne HFHSSWR, considering its inherent challenges of low measurement accuracy, limited detection probability, and ionospheric virtual height stratification perturbations.

The shipborne HFHSSWR and conventional sky-wave HF radar face similar ionospheric challenges. Insights from mature multipath data processing methods in sky-wave HF radar can provide useful guidance. Sky-wave HF radar techniques are typically categorized into three approaches concerning the ionosphere's fixed virtual height: 1) constructing trajectories in radar coordinate systems using established methods like Probabilistic Data Association (PDA) [7], Joint Probabilistic Data Association (JPDA) [8], Multiple Hypothesis Tracker (MHT) [9], and then integrating these

DOI: 10.13164/re.2024.0406

trajectories in Cartesian coordinates through coordinate conversion [10]; 2) employing loop iteration and batch processing methods such as Probabilistic Multiple Hypothesis Tracking (PMHT) [11] and Distributed Expectation-Conditional Maximization (DECM) [12]; and 3) Extending traditional data correlation techniques to multipath conditions by correlating each target propagation mode with measurements, resulting in methods like Multipath PDA (MPDA) [13], Multiple Detection JPDA (MD-JPDA) [14], and Multiple Detection MHT (MD-MHT) [15].

Accurate determination of ionospheric virtual height is critical in radar tracking issue. Common methods such as ionospheric statistical models [16], beacons [17], or ionospheric height detectors [18] are employed, yet regional constraints and the ionosphere's dynamic nature often yield imprecise results. To handle the uncertainty associated with ionospheric virtual height, it is often treated as a random variable based on prior knowledge and incorporated into the target tracking process. Among these approaches, the MPDA for uncertain coordinate registration (MPCR) method [19], which models variations in ionospheric height as a Gaussian noise distribution, is more applicable. However, in practical applications, the variance is often inflated to accommodate ionospheric variations, thereby compromising the accuracy of target state estimation.The multipath data association method employing adaptive multi-model sets introduces multiple ionospheric height models. However, this method's performance heavily depends on the model set selection, and if the chosen set significantly deviates from actual ionospheric variations, the algorithm's efficacy diminishes [20]. The distributed expectation maximization method jointly estimates ionospheric altitude and target state, primarily addressing fixed ionospheric virtual altitudes, leading to initial measurement biases and disregarding the ionosphere's time-varying nature [12].

It is necessary to take into account the time-varying effect of the ionospheric height on the radar measurement error in a nuanced way. The effect of ionospheric height on radar measurement error varies from location to location, resulting in a time-varying radar measurement error. The time-varying effects of ionospheric height variations on radar measurement error, as well as the problem of sea clutter expansion due to the motion of the shipboard platform affecting target bearing estimation accuracy, can be effectively modeled using variational Bayesian inference. The method is widely used in different fields such as combined navigation [21] and airborne radar [22], and is capable of estimating the target state under time-varying measurement noise conditions, which is useful in complex operational environments.

In this study, to address the multipath effects caused by ionospheric stratification in shipborne HFHSSWR radar, we introduced a multi-detection model. This model was employed to form fused measurements using the multipath information, thereby enhancing the actual detection probability of targets. To address unknown and time-varying ionospheric virtual heights caused by the shipborne platform's motion and inaccurate azimuth error parameter settings, we proposed using variational Bayes to analyze the fused measurements' noise covariance matrix based on the MPCR method. This enables more precise state estimation and effectively enhances the target tracking capability of shipborne HFHSSWR. The study unfolds in the following manner: Section 2 models the shipborne HFHSSWR and delineates the associated challenges; Section 3 introduces a multipath target tracking method grounded in variational Bayesian inference; and Section 4 conducts rigorous simulations to validate the efficacy of the proposed method. Finally, the paper encapsulates the research outcomes, summarizing the valuable insights garnered throughout the study.

2. Modelling

In this section, we present the target motion model and the measurement model of the shipborne HFHSSWR. Additionally, we delve into a detailed discussion regarding the impact of ionospheric virtual height on radar measurements.

2.1 Target Motion Model

The state of the target in the 2 Dimensional (2D) Cartesian coordinate system at moment k is $\mathbf{X}(k) = [x_k\ y_k\ \dot{x}_k\ \dot{y}_k]$, where x_k and $\dot{x}_k$ denote the position and velocity on the x-axis, and y_k and $\dot{y}_k$ represent the position and velocity on the y-axis, respectively. The motion model of the target is then expressed as:

$$\mathbf{X}(k) = \mathbf{F}\mathbf{X}(k-1) + \mathbf{v}(k) \tag{1}$$

where the state transfer matrix $\mathbf{F}$ as:

$$\mathbf{F} = \begin{bmatrix} 1 & T_\mathrm{s} & 0 & 0 \\ 0 & 1 & 0 & 0 \\ 0 & 0 & 1 & T_\mathrm{s} \\ 0 & 0 & 0 & 1 \end{bmatrix} \tag{2}$$

where T_s is the sampling time interval, and $\mathbf{v}(k)$ is the process noise with covariance $\mathbf{Q}(k)$:

$$\mathbf{Q}(k) = \begin{bmatrix} T_\mathrm{s}^4\sigma_\mathrm{v}^2/4 & 0 & T_\mathrm{s}^3\sigma_\mathrm{v}^2/2 & 0 \\ 0 & T_\mathrm{s}^4\sigma_\mathrm{v}^2/4 & 0 & T_\mathrm{s}^3\sigma_\mathrm{v}^2/2 \\ T_\mathrm{s}^3\sigma_\mathrm{v}^2/2 & 0 & T_\mathrm{s}^2\sigma_\mathrm{v}^2 & 0 \\ 0 & T_\mathrm{s}^3\sigma_\mathrm{v}^2/2 & 0 & T_\mathrm{s}^2\sigma_\mathrm{v}^2 \end{bmatrix} \tag{3}$$

where σ_v is the process noise variance in the form of acceleration.

2.2 Measurement Model

In this paper, the radar observation model is shown in Fig. 1.

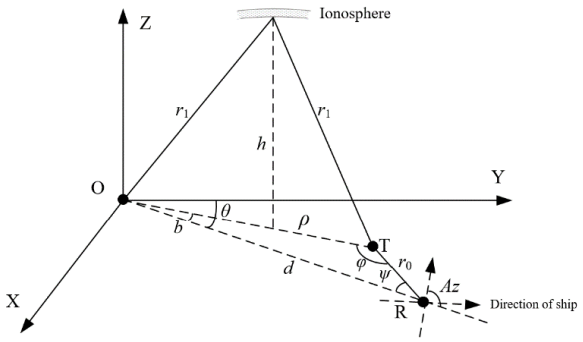

Fig. 1. Measurement model of shipborne HFHSSWR.

The 3 Dimensional (3D) Cartesian coordinate system is defined with the transmitter serving as the origin O and is approximated within a planar model. In this system, the x-axis indicates the east direction, the y-axis represents the north direction, and the z-axis signifies the sky direction. Within this framework, the state of the shipborne platform R in the coordinate system is denoted as $[x_\mathrm{r}\ y_\mathrm{r}\ \dot{x}_\mathrm{r}\ \dot{y}_\mathrm{r}]$, while the state of the target T is expressed as $[x_\mathrm{t}\ y_\mathrm{r}\ \dot{x}_\mathrm{r}\ \dot{y}_\mathrm{r}]$. The distance between the transmitter and the receiver is denoted as d, and the heights of the E and the F ionospheres are respectively indicated by h_E and h_F. Furthermore, the transmitter-target path length is represented as ρ. The angle ψ and ϕ respectively represent the angles between the paths from the transmitter to the receiver and from the receiver to the target, and between the paths from the transmitter to the target and from the receiver to the target. Lastly, Az signifies the angle between the receiver method on the shipborne platform and the path from the target to the receiver. It is noteworthy that all angles in this paper are positive, following a clockwise rotation, and fall within the range $[0, 2\pi)$.

The vector between the target and the transmitter is denoted as $\vec{v}$, with θ_TR representing the angle between the positive x-axis direction and $\vec{v}$. Furthermore, θ_vR signifies the angle between the bow direction and the positive x-axis, and θ_R represents the angle between the line connecting the transmitter and the target and the positive x-axis. Radar signals propagate in two single-hop modes: E-layer reflections and F-layer reflections, each with probabilities of detection denoted as p_d^E and p_d^F, the radar measurement model is $\mathbf{Z}(k) = [Rg,\ D,\ Az]$, encompassing radial distance, Doppler velocity, and azimuth. Notably, the false ionospheric height influences radial distance and Doppler velocity but not azimuth angle, rendering the azimuth angle consistent for both propagation modes:

$$Az = \theta_\mathrm{vR} + \theta_\mathrm{vR} - \pi/2. \tag{4}$$

The radial distances for the two propagation modes are:

$$\begin{aligned} Rg_m =& \sqrt{x_\mathrm{t}^2 + y_\mathrm{t}^2 + 4h_m^2} \\ &+ \sqrt{(x_\mathrm{r} - x_\mathrm{t})^2 + (y_\mathrm{r} - y_\mathrm{t})^2}, \quad m = E, F. \end{aligned} \tag{5}$$

For convenience in subsequent derivations, we have defined two intermediate variables:

$$\begin{aligned} r_0 &= \sqrt{(x_\mathrm{r} - x_\mathrm{t})^2 + (y_\mathrm{r} - y_\mathrm{t})^2}, \\ r_1 &= \sqrt{x_\mathrm{t}^2 + y_\mathrm{t}^2 + 4h_m^2}, \quad m = E, F. \end{aligned} \tag{6}$$

Similarly, the Doppler velocities in both modes of propagation are:

$$\begin{aligned} D_m =& \frac{x_\mathrm{t}\dot{x}_\mathrm{t} + y_\mathrm{t}\dot{y}_\mathrm{t}}{\sqrt{x_\mathrm{t}^2 + y_\mathrm{t}^2 + 4h_m^2}} \\ &+ \frac{(x_\mathrm{r} - x_\mathrm{t})\,(\dot{x}_\mathrm{r} - \dot{x}_\mathrm{t}) + (y_\mathrm{r} - y_\mathrm{t})\,(\dot{y}_\mathrm{r} - \dot{y}_\mathrm{t})}{\sqrt{(x_\mathrm{r} - x_\mathrm{t})^2 + (y_\mathrm{r} - y_\mathrm{t})^2}}. \end{aligned} \tag{7}$$

2.3 Effects of the Ionosphere

As shown in Sec. 2.2, similar to the modeling in skywave over-the-horizon radar, we approximate the ionosphere as a mirror and simplify our study by assuming the ionospheric height as a random variable. Additionally, it can be observed that the virtual height of the ionosphere is an important parameter in the coordinate transformation. Shipborne HFHSSWR distance and Doppler velocity in both propagation modes are affected by the height of the ionosphere, taking the mth ionosphere as an example, at this time, the mth ionosphere height error is Δh_m, $m = E, F$, and the distance can be reconstructed as:

$$\begin{aligned} \tilde{R}g_m =& \sqrt{x_\mathrm{t}^2 + y_\mathrm{t}^2 + 4(h_m + \Delta h_m)^2} \\ &+ \sqrt{(x_\mathrm{r} - x_\mathrm{t})^2 + (y_\mathrm{r} - y_\mathrm{t})^2}. \end{aligned} \tag{8}$$

And the Doppler velocity:

$$\begin{aligned} \tilde{D}_m =& \frac{x_\mathrm{t}\dot{x}_\mathrm{t} + y_\mathrm{t}\dot{y}_\mathrm{t}}{\sqrt{x_\mathrm{t}^2 + y_\mathrm{t}^2 + 4(h_m + \Delta h_m)^2}} \\ &+ \frac{(x_\mathrm{r} - x_\mathrm{t})\,(\dot{x}_\mathrm{r} - \dot{x}_\mathrm{t}) + (y_\mathrm{r} - y_\mathrm{t})\,(\dot{y}_\mathrm{r} - \dot{y}_\mathrm{t})}{\sqrt{(x_\mathrm{r} - x_\mathrm{t})^2 + (y_\mathrm{r} - y_\mathrm{t})^2}}. \end{aligned} \tag{9}$$

The error of the ionospheric height for the distance at this point is:

$$\begin{aligned} \Delta Rg_m &= Rg_m - \tilde{R}g_m \\ &= \frac{-4\Delta h\,(2h + \Delta h)}{\sqrt{x_\mathrm{t}^2 + y_\mathrm{t}^2 + 4(h_m + \Delta h_m)^2} + \sqrt{x_\mathrm{t}^2 + y_\mathrm{t}^2 + 4(h_m)^2}}. \end{aligned} \tag{10}$$

And the Doppler velocity:

$$\begin{aligned} \Delta D_m &= D_m - \tilde{D}_m \\ &= \frac{-\Delta R_m\,(x_\mathrm{t}\dot{x}_\mathrm{t} + y_\mathrm{t}\dot{y}_\mathrm{t})}{\sqrt{x_\mathrm{t}^2 + y_\mathrm{t}^2 + 4(h_m)^2}\sqrt{x_\mathrm{t}^2 + y_\mathrm{t}^2 + 4(h_m + \Delta h_m)^2}}. \end{aligned} \tag{11}$$

Equations (10) and (11) reveal that the impact of ionospheric altitude error on radial distance and Doppler velocity isn't solely dependent on ionospheric altitude and its error. It's intricately linked to the target's position and velocity information in the coordinate system. Consequently, even if the ionospheric altitude error remains constant, the radar measurement error is still time-varying. Ionospheric heights are typically detected using an ionosonde. However, due to objective factors, ionosondes may only be deployed in available regions. For areas without an ionosonde, prior values are determined based on historical data from the ionospheric model. We adopt the approach from reference [19], where the ionospheric altitude model is structured as a Gaussian distribution. The mean value of the mth layer of the ionosphere is denoted as $\hat{h}_m$, and the variance is represented as σ_m. Subsequently, the measurement conversion equation can be formulated as follows:

$$\mathbf{Z}_m(k) = \mathbf{H}\left(\mathbf{X}(k); \hat{h}_m, \sigma_m\right) + \mathbf{w}_m(k) \tag{12}$$

where $\mathbf{w}_m(k)$ is zero-mean non-Gaussian noise, at which point the measurement noise can be rewritten as:

$$\mathbf{R}_m(\mathbf{x}(k); \hat{\mu}) = \operatorname{cov}(\mathbf{w}_m(k)) = \mathbf{R}_\mathrm{s} + \mathbf{R}_\mathrm{cr}^m(k) \tag{13}$$

where $\mathbf{R}_\mathrm{s}$ is the measurement noise, $\mathbf{R}_\mathrm{cr}^m(k)$ is the ionospheric random perturbation noise, $\mathbf{R}_\mathrm{cr}^m(k) = \mathbf{H}_\mathrm{h}^m(k)\,\sigma_m^2\left(\mathbf{H}_\mathrm{h}^m(k)\right)^\mathrm{T}$, $\mathbf{H}_\mathrm{h}^m(k)$ is derived under the planar measurement model of shipborne HFHSSWR already established above:

$$\mathbf{H}_\mathrm{h}^m(k) = \frac{\mathrm{d}\mathbf{Z}}{\mathrm{d}h} = \begin{bmatrix} \frac{2h_m}{r_0} \\ 0 \\ -\frac{x_\mathrm{t}v_{x\mathrm{t}}+y_\mathrm{t}v_{y\mathrm{t}}}{2{r_0}^3} \end{bmatrix}. \tag{14}$$

The derived $\mathbf{R}_m$ using the aforementioned method is equivalent to extending the Gaussian measurement noise $\mathbf{R}_\mathrm{s}$ to non-Gaussian measurement noise based on the provided ionospheric altitude model. This expansion widens the gate range, ensuring that abrupt shifts in measurement values caused by ionospheric altitude transformations fall within the gate range. However, this approach raises two crucial issues:

1) To ensure that measurement points affected by abrupt ionospheric altitude changes fall within the gate range, the set variance σ_m of ionospheric virtual height is typically larger than the actual variance. However, due to the fluctuation in ionospheric virtual height, part of the time experiences a smaller variance than the set virtual height variance. This variation impacts the accurate estimation of the target state under changing ionospheric altitudes;

2) The actual variation in ionospheric virtual height does not precisely align with the Gaussian distribution, leading to disparities between the $\mathbf{R}_m$ formed by the aforementioned method and the actual error matrix. This mismatch further impacts the estimation of the target state during fluctuations in ionospheric height.

Therefore, it is imperative to account for scenarios where the impact of ionospheric virtual height on the measurement noise matrix is unknown. Addressing this uncertainty is essential for enhancing tracking accuracy in the aforementioned context.

3. Data Association Methods Based on Variational Bayesian Inference

The target tracking method proposed in this paper is structured in two steps: In the initial phase, measurements are selected utilizing the established model and an extended gate; the subsequent step involves the fusion of measurement traces. A measurement group is constructed for the fused E and F layer measurement traces. The variational Bayesian method is employed to reason about the error covariance matrix, leading to a significant enhancement in tracking accuracy.

3.1 Measurement Group Construction

The shipborne HFHSSWR employs a hybrid coordinate system for target tracking. Prior to data correlation, it is essential to predict the target state and establish the correlation gate by selecting measurements within the gate. This aspect of HFHSSWR involves deriving the method for selecting measurements.

Prediction of the target state, at this time the target state of the one-step prediction value is:

$$\mathbf{X}(k\,|k-1) = \mathbf{F}\mathbf{X}(k-1). \tag{15}$$

According to (4)–(7), $\mathbf{X}(k\,|k-1)$ can be converted into the measured one-step prediction value $\mathbf{Z}_m(k\,|k-1) = [Rg_m, D_m, A]$ in the radar coordinate system, and the gate can be established with $\mathbf{Z}_m(k\,|k-1)$, as the centre to establish the gate, the mth mode gate:

$$\begin{aligned}&\mathbf{G}_m(k+1) = \\ &[\mathbf{z}(k) - \mathbf{Z}_m(k|k-1)]'\,\mathbf{S}_m(k)^{-1}\,[\mathbf{z}(k) - \mathbf{Z}_m(k|k-1)]\end{aligned} \tag{16}$$

where $\mathbf{z}(k)$ is the k-moment measure and $\mathbf{S}_m(k)$ is the new interest covariance of the mth mode:

$$\mathbf{S}_m(k) = \mathbf{H}_m(k)\,\mathbf{P}(k|k-1)\,\mathbf{H}_m'(k) + \mathbf{R}_m(k) \tag{17}$$

where $\mathbf{P}(k|k-1)$ is the one-step prediction of the target state error covariance at moment k, with $\mathbf{P}(k-1|k-1)$ as the state error covariance at moment $k-1$:

$$\mathbf{P}(k|k-1) = \mathbf{F}\mathbf{P}(k-1|k-1)\,\mathbf{F}' + \mathbf{Q}(k). \tag{18}$$

In (17), $\mathbf{H}_m(k)$ is:

$$\mathbf{H}_m = \frac{\mathrm{d}\mathbf{Z}}{\mathrm{d}\mathbf{X}'} = \begin{bmatrix} H_{11} & 0 & H_{13} & 0 \\ H_{21} & H_{22} & H_{23} & H_{24} \\ H_{31} & 0 & H_{33} & 0 \end{bmatrix}, \tag{19}$$

$$\begin{cases} H_{11}=\frac{x_t}{r_0}-\frac{x_r-x_t}{r_1}, H_{13}=\frac{y_t}{r_0}-\frac{y_r-y_t}{r_1}, \\ H_{22}=\frac{x_t}{r_0}-\frac{x_r-x_t}{r_1}, H_{24}=\frac{y_t}{r_0}-\frac{y_r-y_t}{r_1}, \\ H_{21}=\frac{y_t^2\dot{x}_t-x_ty_t\dot{y}_t+4h_m^2\dot{x}_t}{r_0^3} \\ -\frac{(y_r-y_t)^2(\dot{x}_r-\dot{x}_t)-(x_r-x_t)(y_r-y_t)(\dot{y}_r-\dot{y}_t)}{r_1^3}, \\ H_{23}=\frac{x_t^2\dot{y}_t-x_ty_t\dot{x}+4h_m^2\dot{y}_t}{r_0^3} \\ -\frac{(x_r-x_t)^2(\dot{y}_r-\dot{y}_t)-(x_r-x_t)(y_r-y_t)(\dot{x}_r-\dot{x}_t)}{r_1^3}, \\ H_{31}=\frac{y_r-y_t}{r_1^2}, H_{33}=\frac{x_t-x_r}{r_1^2}. \end{cases} \tag{20}$$

The total gate range is then the concatenation of the individual propagating gates:

$$\mathbf{G}(k)=\bigcup_m \mathbf{G}_m(k). \tag{21}$$

For shipborne HFHSSWR, take E-layer gate and F-layer gate as an example, at this time the relationship between the measurement and the gate is shown in Fig. 2.

The measures falling into the E-layer gate at moment k are z_1, z_2, and those falling into the F-layer gate are z_2, z_3, then groups of measures can be formed depending on the choice of measures, and $q(q <= n)$ measures can be selected to be associated with $n = 2$ propagation modes from $q(k) = 3$ measures, where the E-layer association is z_{E} and the F-layer association is z_{F}.

1) When one measurement is associated, the measurement group is: $z_{\mathrm{E}} = z_1$, $z_{\mathrm{E}} = z_2$, $z_{\mathrm{F}} = z_2$, $z_{\mathrm{F}} = z_3$;

2) When two measurements are associated, the measurement group is: $z_{\mathrm{E}} = z_1, z_{\mathrm{F}} = z_2$, $z_{\mathrm{E}} = z_2, z_{\mathrm{F}} = z_3$, $z_{\mathrm{F}} = z_2, z_{\mathrm{F}} = z_3$.

Measurement groups can be defined according to φ and n_φ, and the measurement group z_{φ,n_φ} represents the n_φth measurement group that selects φ measurements, when $\varphi = 1$ and $n_\varphi = 1$, at this time, the measurement group z_{φ,n_φ} represents $[z_1(k)]$ and constructs the relevant events as $\theta_{\varphi,n_\varphi}(k)$, $n_\varphi = 0$ for no measurements originating from the target,and when there are φ measures originating from the target, $n_\varphi = 1, 2, \cdots, C_{q_k}^{\varphi}$ where $C_{m(k)}^{\varphi}$ denotes the number of combinations to select φ out of the q_k measurement traces.

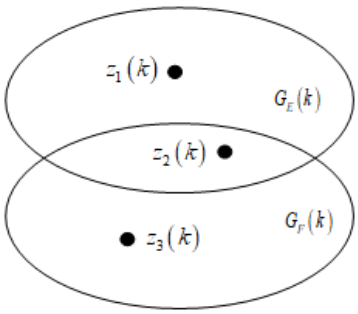

Fig. 2. Schematic diagram of a gate.

3.2 Fusion of Measurement Groups

The conditional probability that the measure group z_{φ,n_φ} originates from the target, as described in Sec. 3.1, is:

$$\begin{aligned}\beta_{\varphi,n_\varphi}(k)=&\frac{1}{c}p\left(\mathbf{Z}^k\left|\theta_{\varphi,n_\varphi}(k),q(k),\varphi,\mathbf{Z}^{k-1}\right.\right)\\&\times p\left(\theta_{\varphi,n_\varphi}(k)\left|q(k),\varphi,\mathbf{Z}^{k-1}\right.\right)\end{aligned} \tag{22}$$

where c is the normalisation factor and $\mathbf{Z}^k$ denotes the cumulative set of confirmed measurements up to the kth moment. The above equation can be split into a probability density function and a conditional probability calculation at the relevant time, where the probability density function is:

$$\begin{aligned}&p\left(\mathbf{Z}^k\left|\theta_{\varphi,n_\varphi}(k),q(k),\varphi,\mathbf{Z}^{k-1}\right.\right)\\&=\begin{cases}\frac{\mathbf{G}(k)^{-q(k)+\varphi}}{P_{\mathrm{G}}}N\left(\mathbf{v}_{\varphi,n_\varphi}(k);0,\mathbf{S}_{\varphi,n_\varphi}(k)\right), \\ \qquad n_\varphi=1,\cdots,C_{q(k)}^{\varphi} \\ \mathbf{G}(k)^{-q(k)}, \quad n_\varphi=0\end{cases}\end{aligned} \tag{23}$$

where P_{G} is the gate coefficient, $N(\bullet)$ denotes the likelihood function, $\mathbf{v}_{\varphi,n_\varphi}(k)$ and $\mathbf{S}_{\varphi,n_\varphi}(k)$ are the new interest and new interest covariance of the measurement group $\mathbf{z}_{\varphi,n_\varphi}$, respectively, where $\mathbf{v}_{\varphi,n_\varphi}(k)$ is:

$$\mathbf{v}_{\varphi,n_\varphi}(k)=\begin{bmatrix}\left(\mathbf{z}_1(k)-\mathbf{Z}_1(k|k-1)\right)'\\ \vdots \\ \left(\mathbf{z}_\varphi(k)-\mathbf{Z}_\varphi(k|k-1)\right)'\end{bmatrix}, \tag{24}$$

$$\begin{aligned}\mathbf{S}_{\varphi,n_\varphi}(k)=&\mathbf{H}_{\varphi,n_\varphi}(k)\mathbf{P}(k|k-1)\mathbf{H}_{\varphi,n_\varphi}(k)'\\&+\mathbf{R}_{\varphi,n_\varphi}(k)\end{aligned} \tag{25}$$

where
$$\mathbf{H}_{\varphi,n_\varphi}(k)=\left[\mathbf{H}_1(k),\cdots,\mathbf{H}_\varphi(k)\right]' \tag{26}$$

and $\mathbf{R}_{\varphi,n_\varphi}(k)$ is:

$$\mathbf{R}_{\varphi,n_\varphi}(k)=\begin{bmatrix}\mathbf{R}_1(k) & 0 & \cdots & 0\\ \vdots & \mathbf{R}_2(k) & \cdots & 0\\ \vdots & \vdots & \ddots & \vdots\\ 0 & 0 & \cdots & \mathbf{R}_\varphi(k)\end{bmatrix}. \tag{27}$$

Then the conditional probability of the event in question is:

$$\begin{aligned}&p\left(\theta_{\varphi,n_\varphi}(k)\left|q(k),\varphi,\mathbf{Z}^{k-1}\right.\right)=\\&\begin{cases}\frac{1}{q(k)}\frac{P_{\mathrm{D}_\varphi}P_{\mathrm{G}}u(q(k)-\varphi)}{\sum_{\varphi=1}^{q(k)}P_{\mathrm{D}_\varphi}P_{\mathrm{G}}u(q(k)-\varphi)+(1-P_{\mathrm{D}}P_{\mathrm{G}})u(q(k))}, \\ \qquad n_\varphi=1,\cdots,C_{q(k)}^{\varphi} \\ \frac{(1-P_{\mathrm{D}}P_{\mathrm{G}})u(q(k))}{\sum_{\varphi=1}^{q(k)}P_{\mathrm{D}_\varphi}P_{\mathrm{G}}u(q(k)-\varphi)+(1-P_{\mathrm{D}}P_{\mathrm{G}})u(q(k))}, \\ \qquad n_\varphi=0\end{cases}\end{aligned} \tag{28}$$

where $u(\bullet)$ is the probability mass function of the number of false measurements, and P_{D_φ} is the probability that the target φ propagation modes are all able to be detected, when the total probability that the target is detected is:

$$P_{\mathrm{D}}=\sum_{\varphi=1}^{\varphi_{\max}}P_{\mathrm{D}_\varphi}. \tag{29}$$

This effectively enhances the target detection probability. Assuming the detection probability for a single path is 0.6, integrating the detection probabilities from two paths yields a discovery probability of 0.84, which is an improvement of 0.24 over the detection probability of a single path.

For the measure group $\mathbf{z}_{\varphi,n_\varphi}$, if there is a propagation path not associated with the measure value, the predicted value of the one-step measure is used as the measure value, otherwise the associated measure is used directly as the measure value, forming a reconstructed measure group $\tilde{\mathbf{z}}_{\varphi,n_\varphi}$, and according to the reconstructed measure group and the conditional probability of obtaining the fusion measure group:

$$\tilde{\mathbf{Z}}\left(k|k\right)=\sum_{\varphi=1}^{\varphi_{\max}}\sum_{n_\varphi=1}^{C_{m(k)}^{\varphi}}\beta_{\varphi,n_\varphi}\left(k\right)\tilde{\mathbf{z}}_{\varphi,n_\varphi}. \tag{30}$$

3.3 Variational Bayesian Inference

In the Kalman filtering method, measurement noise covariance is typically modeled as zero-mean Gaussian distributed noise, with the target state estimated using the minimum mean square approach. In practical environments, due to the potential for sea clutter to obscure the target caused by sea conditions and ship motion, the azimuth measurement error is often set to a larger value to maintain trajectory continuity. As discussed in Sec. 2.3, the effect of ionospheric altitude on the target can be incorporated into the time-varying measurement noise covariance, so we can associate the errors in the radar measurements with the errors in the ionospheric altitude variations in a unified measurement error matrix, which can be approximated by using the measurements to approximate this measurement error matrix. This allows us to comprehensively consider the effects of time-varying azimuth error and ionospheric height on the actual processing. By adjusting the parameters in the processing, including ionospheric height error and azimuth setting error, we ensure the continuity of the target trajectory. The variational Bayes method is employed to approximate the true measurement noise covariance matrix. In this section, we employ variational Bayesian inference on this measurement error matrix. By doing so, we obtain a covariance approximation that closely aligns with the actual measurement noise. This technique significantly enhances the accuracy of target state estimation.

The inverse gamma distribution is taken to update the measurement noise covariance, at which time the measurement noise covariance matrix $\tilde{\mathbf{R}}\left(k\right)$ and the target state $\mathbf{X}\left(k\,|k\right)$ are both estimated measurements, at which time the posterior probability given by the fused set of measurements can be approximated as:

$$p\left(\mathbf{X}\left(k\,|k\right),\tilde{\mathbf{R}}\left(k\right)|\tilde{\mathbf{Z}}^{k}\right)\approx q\left(\mathbf{X}\left(k\,|k\right)\right)q\left(\tilde{\mathbf{R}}\left(k\right)\right). \tag{31}$$

In order to maximize the degree of approximation, the KL dispersion needs to be minimised, both:

$$\arg\min\int q\left(\mathbf{X}\left(k\,|k\right)\right)q\left(\tilde{\mathbf{R}}\left(k\right)\right)\frac{q\left(\mathbf{X}\left(k\,|k\right)\right)q\left(\tilde{\mathbf{R}}\left(k\right)\right)}{p\left(\mathbf{X}\left(k\,|k\right),\tilde{\mathbf{R}}\left(k\right)|\tilde{\mathbf{Z}}^{k}\right)}. \tag{32}$$

According to the literature [16] the optimal solution of (32) can be obtained as:

$$\log q\left(\theta\right)=E_{\Theta^{-\theta}}\left[\log p\left(\Theta,\mathbf{Z}^{k}\right)\right]+c_\theta \tag{33}$$

where $\Theta\triangleq\left\{\mathbf{X}\left(k\,|k\right),\tilde{\mathbf{R}}\left(k\right)\right\}$ and $E_{\Theta^{-\theta}}\left[\bullet\right]$ denotes the expectation of the parameters other than the parameter θ, and c_θ is a constant term containing θ. However, $q\left(\mathbf{X}\left(k\,|k\right)\right)$ and $q\left(\tilde{\mathbf{R}}\left(k\right)\right)$ are coupled to each other, and thus Equation (33) can be solved iteratively:

$$\begin{aligned}p\left(\Theta,\mathbf{Z}^{k}\right)&=p\left(\tilde{\mathbf{R}}\left(k\right)\left|\mathbf{Z}^{k-1}\right.\right)p\left(\mathbf{Z}^{k-1}\right)\\&\quad\times p\left(\mathbf{Z}\left(k\right)\left|\mathbf{X}\left(k\,|k\right),\tilde{\mathbf{R}}\left(k\right)\right.\right)p\left(\mathbf{X}\left(k\,|k\right)\left|\mathbf{Z}^{k-1}\right.\right).\end{aligned} \tag{34}$$

At this time, the inverse gamma distribution is adopted as the conjugate prior distribution of the variance of the Gaussian distribution [23], at this time, the probability distribution function of $\tilde{\mathbf{R}}\left(k\right)$ consists of α_k^-,β_k^-, at this time, $\tilde{\mathbf{R}}\left(k\right)=\mathrm{diag}\left(\tilde{\mathbf{R}}_1\left(k\right),\tilde{\mathbf{R}}_2\left(k\right),\cdots,\tilde{\mathbf{R}}_i\left(k\right),\cdots,\tilde{\mathbf{R}}_d\left(k\right)\right)$, d is the number of dimensions of $\tilde{\mathbf{R}}\left(k\right)$, and according to the fusion of quantitative measurement group in Sec. 3.2, it can be obtained that d is 6:

$$\begin{aligned}&\mathrm{Inv-Gamma}\left(\tilde{\mathbf{R}}_i\left(k\right)\right)=\\&\frac{\left(\beta_{k,i}^-\right)^{\alpha_{k,i}^-}}{\Gamma\left(\alpha_{k,i}^-\right)}\left(\tilde{\mathbf{R}}_i\left(k\right)\right)^{-\alpha_k^--1}\exp\left(-\frac{\beta_{k,i}^-}{\tilde{\mathbf{R}}_i\left(k\right)}\right),\\&\Gamma\left(\delta\right)=\int_0^\infty g^{\delta-1}\mathrm{e}^{-g}\mathrm{d}g,\end{aligned} \tag{35}$$

$$\begin{aligned}p\left(\Theta,\mathbf{Z}^{k}\right)&=N\left(\mathbf{Z}\left(k\right);\mathbf{H}\left(k\right)\mathbf{X}\left(k\,|k\right),\tilde{\mathbf{R}}\left(k\right)\right)\\&\quad\times\sum_{i=1}^{d}\mathrm{Inv-Gamma}\left(\tilde{\mathbf{R}}_i\left(k\right)\left|\sigma_{k,i}^-,\beta_{k,i}^-\right.\right)\\&\quad\times N\left(\mathbf{X}\left(k|k\right);\mathbf{X}\left(k\,|k-1\right),\mathbf{P}\left(k|k-1\right)\right)\\&\quad\times p\left(\mathbf{Z}^{k-1}\right),\end{aligned} \tag{36}$$

$$\begin{aligned}\log p\left(\Theta,\mathbf{Z}^{k}\right)&=\sum_{i=1}^{d}-0.5(\mathbf{Z}\left(k\right)-\mathbf{H}\left(k\right)\mathbf{X}\left(k\,|k\right))^2\tilde{\mathbf{R}}_i(k)^{-1}\\&\quad-\frac{\beta_{k,i}^-}{\tilde{\mathbf{R}}_i\left(k\right)}-\left(\alpha_{k,i}^-+\frac{3}{2}\right)\log\tilde{\mathbf{R}}_i\left(k\right)\\&\quad-0.5\varpi^{\mathrm{T}}\mathbf{P}\left(k|k-1\right)\varpi+c_\Theta,\end{aligned} \tag{37}$$

and

$$\varpi=\mathbf{X}\left(k\,|k\right)-\mathbf{X}\left(k\,|k-1\right). \tag{38}$$

When the parameter $\theta = \tilde{\mathbf{R}}_i(k)$, the joint solution of (38) and (33) can be obtained:

$$\begin{aligned}&\log q\left(\tilde{\mathbf{R}}_i(k)\right)\\&=\sum_{i=1}^{d}-0.5E\left(\left(\mathbf{Z}(k)-\mathbf{H}(k)\mathbf{X}(k|k)\right)^2\right)\tilde{\mathbf{R}}_i(k)^{-1}\\&-\frac{\beta_{k,i}^-}{\tilde{\mathbf{R}}_i(k)}+\left(\alpha_{k,i}^-+\tfrac{3}{2}\right)\log\tilde{\mathbf{R}}_i(k)\\&-0.5E\left(\varpi^{\mathrm{T}}\mathbf{P}(k|k-1)^{-1}\varpi\right)+c_\Theta.\end{aligned}\tag{39}$$

The simplification can be obtained:

$$\begin{aligned}&\log q\left(\tilde{\mathbf{R}}_i(k)\right)\\&=\sum_{i=1}^{d}-0.5E\left(\left(\mathbf{Z}(k)-\mathbf{H}(k)\mathbf{X}(k|k)\right)^2\right)\tilde{\mathbf{R}}_i(k)^{-1}\\&+\left(\alpha_{k,i}^-+\frac{1}{2}+1\right)\log\tilde{\mathbf{R}}_i(k)+c_{\tilde{\mathbf{R}}_i(k)}.\end{aligned}\tag{40}$$

According to (40) the θ after recursive parameter $q\left(\tilde{\mathbf{R}}_i(k)\right)$ is still an inverse gamma distribution, at this point:

$$\begin{aligned}\alpha_{k,i}&=\alpha_{k,i}^{-1}+\frac{1}{2}\\\beta_{k,i}&=\beta_{k,i}^-\\&\quad+\left(\left(\mathbf{Z}(k)-\mathbf{H}(k)\mathbf{X}(k|k)\right)_i\right)^2\\&\quad+\left(\mathbf{H}(k)\mathbf{P}(k|k)\mathbf{H}'(k)\right)_i\end{aligned}\tag{41}$$

and

$$q\left(\tilde{\mathbf{R}}_i(k)\right)=\text{Inv}-\text{Gamma}\left(\tilde{\mathbf{R}}_i(k);\alpha_{k,i},\beta_{k,i}\right).\tag{42}$$

When the parameter $\theta = \mathbf{X}(k|k)$, the joint solution of (37) and (33) can be obtained:

$$\begin{aligned}&\log q\left(\mathbf{X}(k|k)\right)\\&=\sum_{i=1}^{d}-0.5(\mathbf{Z}(k)-\mathbf{H}(k)\mathbf{X}(k|k))^2E\left(\tilde{\mathbf{R}}_i(k)^{-1}\right)\\&-E\left(\frac{\beta_{k,i}^-}{\tilde{\mathbf{R}}_i(k)}\right)+\left(\alpha_{k,i}^-+\tfrac{3}{2}\right)E\left(\log\tilde{\mathbf{R}}_i(k)\right)\\&-0.5\varpi^{\mathrm{T}}E\left(\mathbf{P}(k|k-1)^{-1}\right)\varpi+c_{X(k|k)}.\end{aligned}\tag{43}$$

According to (42):

$$E\left(\tilde{\mathbf{R}}_i(k)^{-1}\right)=\frac{\beta_{k,i}}{\alpha_{k,i}}.\tag{44}$$

Then Equation (43) can be rewritten as:

$$\begin{aligned}\log q\left(\mathbf{X}(k|k)\right)&=\upsilon^{\mathrm{T}}\widehat{\mathbf{R}}(k)^{-1}\upsilon\\&\quad-0.5\varpi^{\mathrm{T}}\mathbf{P}(k|k-1)^{-1}\varpi+c_{\mathbf{X}(k|k)},\end{aligned}\tag{45}$$

$$\upsilon=\mathbf{Z}(k)-\mathbf{H}(k)\mathbf{X}(k|k),\tag{46}$$

$$\widehat{\mathbf{R}}(k)=\text{diag}\left(\beta_{k,1}/\alpha_{k,1},\cdots,\beta_{k,i}/\alpha_{k,i},\cdots,\beta_{k,d}/\alpha_{k,d}\right).\tag{47}$$

Collating (39)–(47) yields single-step variational Bayesian inference:

$$\begin{aligned}\mathbf{X}(k|k)&=\mathbf{X}(k|k-1)\\&\quad+\mathbf{P}(k|k-1)\mathbf{H}(k)^{\mathrm{T}}\left(\mathbf{H}(k)\mathbf{P}(k|k-1)\mathbf{H}(k)^{\mathrm{T}}\right)^{-1}\upsilon,\end{aligned}\tag{48}$$

$$\begin{aligned}\mathbf{P}(k|k)&=\mathbf{P}(k|k-1)\\&\quad-\mathbf{P}(k|k-1)\mathbf{H}(k)^{\mathrm{T}}\left(\mathbf{H}(k)\mathbf{P}(k|k-1)\mathbf{H}(k)^{\mathrm{T}}\right.\\&\quad\left.+\widehat{\mathbf{R}}(k)\right)^{-1}\mathbf{H}(k)\mathbf{P}(k|k-1).\end{aligned}\tag{49}$$

When performing the nth iteration, $\mathbf{X}(k|k-1)$ and $\mathbf{P}(k|k-1)$ can be replaced with the values $\mathbf{X}^{n-1}(k|k)$ and $\mathbf{P}^{n-1}(k|k)$ obtained in the $n-1$st iteration.Also to inherit the parameter values given in the previous moment, set ρ as the forgetting factor, then:

$$\alpha_{k+1,i}=\rho\alpha_{k,i},\beta_{k+1,i}=\rho\beta_{k,i}.\tag{50}$$

3.4 Algorithmic Process

Based on the measurements composed in Sec. 3.2 and the principle of Variational Bayes in Sec. 3.3, the algorithm flow of the shipborne HFHSSWR data correlation method based on variational Bayesian inference proposed in this paper is shown below.

Algorithm 1. Proposed multi-detection-variate Bayesian.

Input:
$\mathbf{X}(k-1|k-1)$, $\mathbf{P}(k-1|k-1)$, $\mathbf{R}_{\mathrm{s}}$, σ_{E}, σ_{F}, ρ, $\mathbf{Z}(k)$
$\beta_{k-1,i}$, $\alpha_{k-1,i}$, $i=1,\cdots,d$
Output:
$\mathbf{X}(k|k)$, $\mathbf{P}(k|k)$, $\beta_{k,i}$, $\alpha_{k,i}$, $i=1,\cdots,d$
Predict: Using (15) and (18), get $\mathbf{X}(k|k-1)$ and $\mathbf{P}(k|k-1)$. Using (4)–(7) to obtain the quantitative predictions in the E and F propagation modes.
Formation of Measurement Group: According to the set ionospheric altitude error σ_{E} and σ_{F}, the gate in E propagation mode and F propagation mode is formed by using (16), and the measurement point traces falling into the gate are formed into measurement groups.
Fusion of Measurement Groups: The fusion of the measurement sets according to (22)–(30) yields the fused measurement set $\tilde{\mathbf{Z}}(k|k)$ and constructs the measurement transformation matrix bcd for the combination of E and F propagation mode measurements.
Initialization: $\mathbf{X}^0(k|k)=\mathbf{X}(k|k-1)$, $\mathbf{P}^0(k|k)=\mathbf{P}(k|k-1)$, $\alpha_{k,i}=0.5+\rho\alpha_{k-1,i},\beta_{k,i}=\rho\beta_{k-1,i}$, $i=1,\cdots,d$. Let N be the maximum number of iterations.
for $n=1:N$ **do**
  $\widehat{\mathbf{R}}^n(k)=\text{diag}\left(\beta_{k,1}/\alpha_{k,1},\beta_{k,2}/\alpha_{k,2},\cdots,\beta_{k,d}/\alpha_{k,d}\right)$
  Using (48)–(50) based on the value of $n-1$st to $\mathbf{X}^n(k|k)$, $\mathbf{P}^n(k|k)$, $\beta_{k,i}^n$
  if $n<N$ **then**
    Reconstruction of the E and F measurement matrices R is performed:
    $\mathbf{R}_{\mathrm{E}}(k)=\text{diag}\left(\beta_{k,1}/\alpha_{k,1},\cdots,\beta_{k,d/2}/\alpha_{k,d/2}\right)$,
    $\mathbf{R}_{\mathrm{F}}(k)=\text{diag}\left(\beta_{k,d/2+1}/\alpha_{k,d/2+1},\cdots,\beta_{k,d}/\alpha_{k,d}\right)$.
    The fusion of the measure sets according to (22)–(30) yields the fused measure set $\tilde{\mathbf{Z}}(k|k)$
  end if
end for

4. Simulation

In order to verify the performance of the above proposed method, simulation is carried out under the shipborne HFHSSWR, and the state of the shipborne platform is set to [10 km, 1 m/s, 1300 km, 55 m/s], the initial state of the target is [100 km, 1 m/s, 1450 km, 4 m/s], the radar detects the clutter at a range of [0, 200 km] on the X-axis and [1300 km, 1500 km] on the Y-axis, and the clutter is poisson distributed in number and uniformly distributed in position, with an expected number of clutter per square kilometer of 0.001 per scanning period. And for the shipborne platform and the target due to the instability of the state of the movement of the noise in the form of the X-axis acceleration and the Y-axis acceleration, which are both consistent with the Gaussian distribution with the mean square deviation of 0.001 m/s^2. In this case, each detection cycle has an accumulation time of 40 s, generating a total of 100 coherent integration time (CIT), and the detection probability of each propagation pathway is set to 0.6.

There are F and E layers in the ionosphere, and the height of the ionosphere in the F layer of the set algorithm is 260 km, and the height of the ionosphere in the E layer is 100 km, the setting of these parameters is consistent with the literature [19]. And at this time, the height of the ionosphere is set as Fig. 3.

The distance error is 1 km, the Doppler error is 0.5 m/s, and the azimuth error is 2°. The method in literature [19] is used as comparison algorithm, at which time the height error in layer E is 10 km, and the height error in layer F is 40 km. And 200 Monte Carlo simulations are performed and the results depicted in Figs. 4–7.

The results demonstrate that the proposed multiple detection variational bayesian PDA (MD-VB-PDA) method exhibits faster convergence compared to the MPCR method in scenarios where ionospheric height is inaccurately set. Moreover, after convergence, the accuracy significantly improves, with enhancements exceeding 10% observed in both X-axis and Y-axis positions and velocities. This outcome substantiates the effectiveness of the proposed method outlined in this paper.

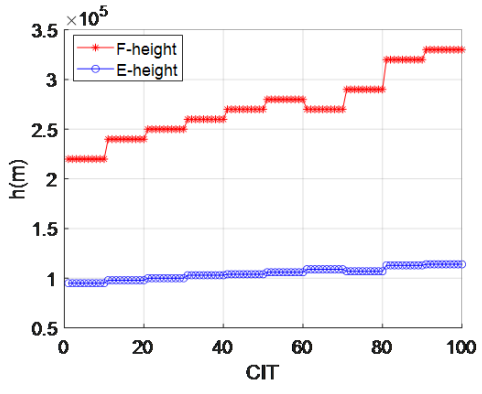

Fig. 3. Ionospheric height setting.

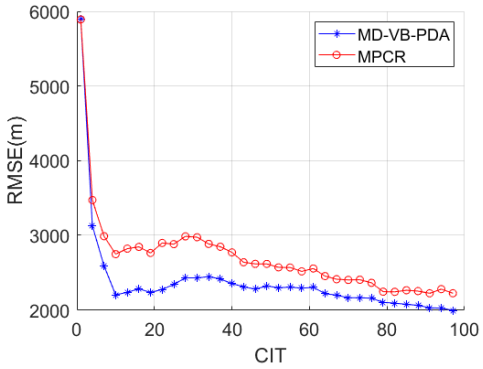

Fig. 4. RMSE comparison for X-axis positions.

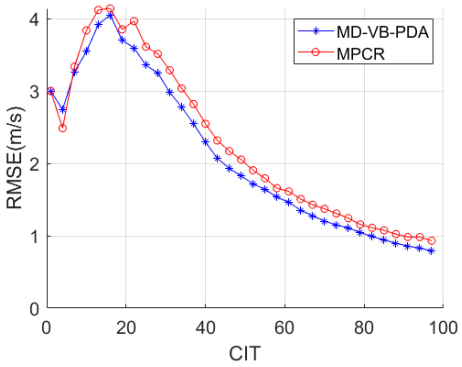

Fig. 5. RMSE comparison for X-axis velocity.

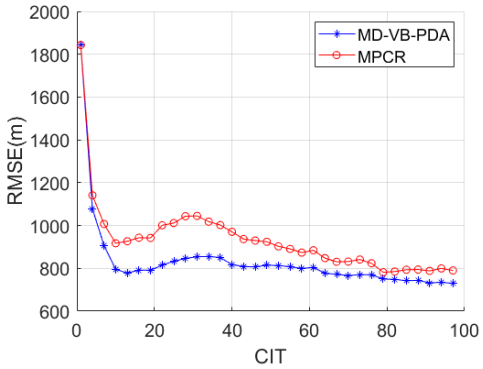

Fig. 6. RMSE comparison for Y-axis positions.

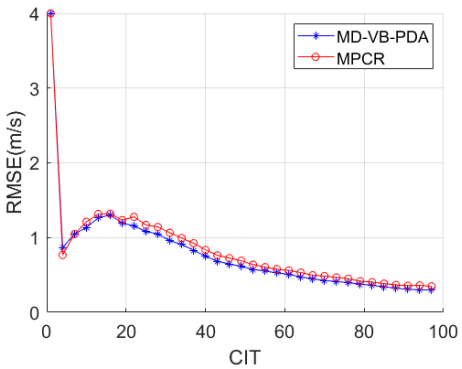

Fig. 7. RMSE comparison for Y-axis velocity.

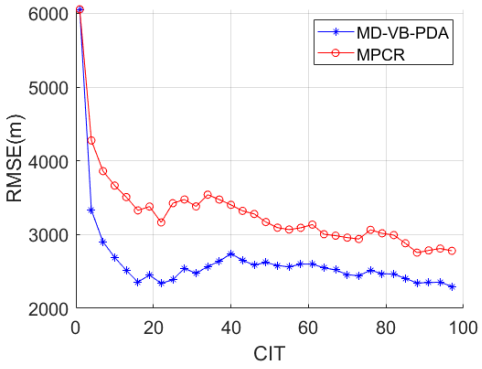

Fig. 8. RMSE comparison for X-axis positions.

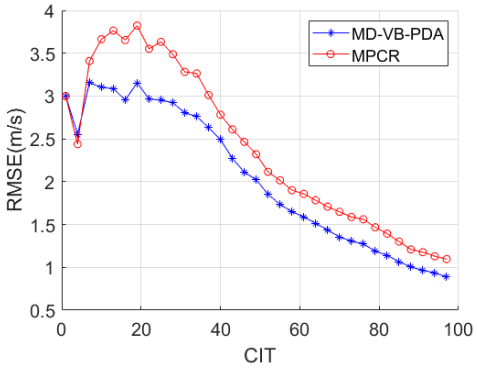

Fig. 9. RMSE comparison for X-axis velocity.

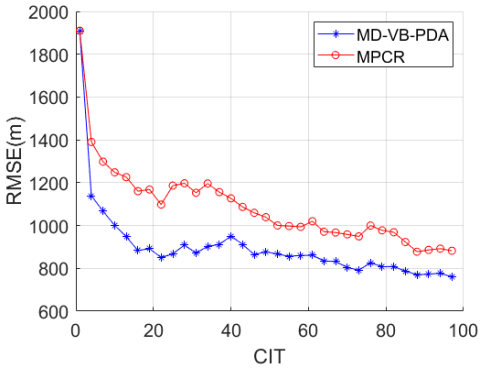

Fig. 10. RMSE comparison for Y-axis positions.

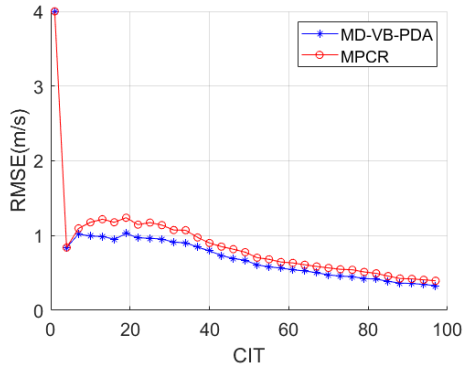

Fig. 11. RMSE comparison for Y-axis velocity.

Similarly, considering the challenge of azimuth error resulting from diverse sea clutter conditions in real detection environments, the algorithm's azimuth error was set at 3° in the aforementioned context. Employing the same methodology, 200 Monte Carlo runs were executed, and the results depicted in Figs. 8–11.

As shown in Figs. 8–11, it can be seen that the method proposed in this paper can improve the performance by more than 15% compared with the traditional method of MPCR when there is a difference between the set azimuthal error and the real azimuthal error and the ionospheric height is inaccurate, and it can effectively overcome the problem of degradation of tracking accuracy of the shipborne high frequency hybrid-surface wave radar due to the ionospheric perturbation and the change of the sea state. The MPCR method models the ionospheric height with a fixed mean and variance, introducing errors from ionospheric height variations into the measurement noise. This amplifies the gating during target tracking predictions, ensuring that the measurements detected by the radar fall within the gating range. Additionally, the azimuth measurement error is considered a constant, leading to an incorrect measurement error covariance matrix $\mathbf{R}_m$. This affects the Kalman gain and results in decreased convergence speed and target estimation accuracy in the MPCR method. The proposed MD-VB-PDA method is conceptually similar to the MPCR method used in skywave over-the-horizon radar for ionospheric height modeling. Based on the derived high-frequency radar detection system model, MD-VB-PDA method calculates the impact of ionospheric height variations on measurement errors. Then, we utilize a multi-detection mode to form fused measurements within the gating range. Using these measurements formed from different paths, the variational Bayes method is employed to approximate the true measurement noise covariance matrix $\widehat{\mathbf{R}}$. By incorporating a measurement error covariance matrix $\widehat{\mathbf{R}}$ closer to the real situation into the filtering process, the Kalman gain is brought closer to the real value, achieving faster convergence speed and higher target accuracy.

5. Conclusion

The shipborne HFHSSWR encounters severe degradation. This is due to the combined influence of the stratified and unstable ionosphere, as well as the movement of the shipborne platforms. As a result, the precision of target trajectories is impacted.This study introduces a novel approach to address this issue, presenting a multi-detection mode tracking method based on variational Bayesian method. For the first time, this method tackles accuracy degradation arising from inaccurate ionospheric height and azimuthal measurement errors caused by sea state. The research begins with an analysis of the impact of ionospheric height error on target tracking within the established shipborne HFHSSWR model, leading to the derivation of a measurement conversion formula.

Subsequently, the variational Bayesian method is integrated into the multi-detection mode. Through measurement fusion and iteration in this mode, the error matrix affected by ionospheric altitude error is updated. Simulation data processing validates the effectiveness of the proposed method, demonstrating its ability to enhance target tracking accuracy even when ionospheric altitude and orientation errors are inaccurately set, the present method is able to improve the tracking accuracy by more than 15%.

This study primarily focuses on single-target tracking under inaccurate ionospheric height and azimuth settings, but there are still some issues that require further investigation. Firstly, extensive research has shown that ionospheric state parameters are spatially correlated, which will aid in subsequently refining the channel model based on the ionospheric model to enhance target tracking capabilities. Secondly, enlarging the gating size may lead to the target entering a multi-target tracking scenario. Future research will mainly address the influence of the ionospheric model on target tracking and multi-target tracking. Error analysis experiments will be conducted using actual measurement data to provide more comprehensive empirical support.

References

[1] ZHU, Y., WEI, Y., YU, L. Ionospheric decontamination for HF hybrid sky-surface wave radar on a shipborne platform. *IEEE Geoscience and Remote Sensing Letters*, 2017, vol. 14, no. 11, p. 2162–2166. DOI: 10.1109/LGRS.2017.2757000

[2] WEI, Y., ZHU, Y. Simulation study of first-order sea clutter Doppler spectra for shipborne high frequency radar via hybrid sky-surface wave propagation. *Applied Remote Sensing*, 2017, vol. 11, no. 1, p. 1–17. DOI: 10.1117/1.JRS.11.014001

[3] ZHU, Y., WEI, Y., TONG, P. Wavefront correction of ionospherically propagated HF radio waves using covariance matching techniques. *Radioengineering*, 2017, vol. 26, no. 1, p. 330–336. DOI: 10.13164/RE.2017.0330

[4] ZHU, Y., WEI, Y., ZHU, K. Sea clutter suppression for shipborne HFSWR using joint sparse recovery-based STAP. *Electronics Letters*, 2016, vol. 52, no. 12, p. 1067–1069. DOI: 10.1049/el.2016.0212

[5] DING, M., TONG, P., WEI, Y., et al. Azimuth resolution improvement and target parameters inversion for distributed shipborne high frequency hybrid sky-surface wave radar. *Remote Sensing*, 2021, vol. 13, no. 13, p. 1–27. DOI: 10.3390/rs13132471

[6] WANG, Z., ZHU, Y., WEI, Y., et al. Cascaded method for ionospheric decontamination and sea clutter suppression for high-frequency hybrid sky-surface wave radar. *IET Signal Processing*, 2015, vol. 9, no. 7, p. 562–571. DOI: 10.1049/iet-spr.2014.0203

[7] BARSHALOM, Y., TSE, E. Tracking in a cluttered environment with probabilistic data association. *IEEE Transactions on Automatic Control*, 1975, vol. 11, no. 5, p. 451–460. DOI: 10.1016/0005-1098(75)90021-7

[8] BARSHALOM, Y., FORTMANN, T., SCHEFFE, T. Sonar tracking of multiple targets using joint probabilistic data association. *IEEE Transactions on Oceanic Engineering*, 1983, vol. 8, no. 3, p. 173–184. DOI: 10.1109/JOE.1983.1145560

[9] DONALD, B. R. An algorithm for tracking multiple targets. *IEEE Transactions on Automatic Control*, 1979, vol. 24, no. 1, p. 843–854. DOI: 10.1109/TAC.1979.1102177

[10] PERCIVAL, D. J., WHITE, K. A. Multihypothesis fusion of multipath over-the-horizon radar tracks. In *Proceedings Volume 3373, Signal and Data Processing of Small Targets*. Orlando (USA), 1998, p. 440–451. DOI: 10.1117/12.324637

[11] LONG, T., ZHENG, L., CHEN, X., et al. Improved probabilistic multi-hypothesis tracker for multiple target tracking with switching attribute states. *IEEE Transactions on Signal Processing*, 2011, vol. 59, no. 12, p. 5721–5733. DOI: 10.1109/TSP.2011.2167616

[12] LAN, H., LIANG, Y., WANG, Z., et al. Distributed ECM algorithm for OTHR multipath target tracking with unknown ionospheric heights. *IEEE Journal of Selected Topics in Signal Processing*, 2018, vol. 12, no. 1, p. 61–75. DOI: 10.1109/JSTSP.2017.2787488

[13] PULFORD, G. W., EVANS, R. J. A multipath data association tracker for over-the-horizon radar. *IEEE Transactions on Aerospace and Electronic Systems*, 1998, vol. 34, no. 4, p. 1165–1183. DOI: 10.1109/7.722704

[14] HABTEMARIAM, B., THARMARASA, R., THAYAPARAN, T., et al. A multiple-detection joint probabilistic data association filter. *IEEE Journal of Setected Topics in Signal Porcessing*, 2013, vol. 7, no. 3, p. 461–471. DOI: 10.1109/JSTSP.2013.2256772

[15] SATHYAN, T., CHIN, T. J., ARULAMPALAM, S., et al. A multiple hypothesis tracker for multitarget tracking with multiple simultaneous measurements. *IEEE Journal of Setected Topics in Signal Porcessing*, 2013, vol. 7, no. 3, p. 448–460. DOI: 10.1109/JSTSP.2013.2258322

[16] BILITZA, D., REINISCH, B. W. International reference ionosphere 2007: Improvements and new parameters. *Advances in Space Research*, 2008, vol. 42, no. 4, p. 599–609. DOI: 10.1016/j.asr.2007.07.048

[17] ZHAO, M., YANG, Q. A new way of estimating ionospheric virtual height based on island multipath echoes in HFSWR. In *IEEE Radar Conference (RadarConf)*. Seattle (WA, USA), 2017, p. 576–580. DOI: 10.1109/RADAR.2017.7944269

[18] WHEADON, N. S., WHITEHOUSE, J. C., MILSOM, J. D., et al. Ionospheric modelling and target coordinate registration for HF sky-wave radars. In *Sixth International Conference on HF Radio Systems and Techniques*. York (UK), 1994, p. 258–266. DOI: 10.1049/cp:19940504

[19] PULFORD, G. W. OTHR multipath tracking with uncertain coordinate registration. *IEEE Transactions on Aerospace and Electronic Systems*, 2004, vol. 40, no. 1, p. 38–56. DOI: 10.1109/TAES.2004.1292141

[20] GUO, L., LAN, J., LI, R. X. Multiple-model approach to over-the-horizon radar tracking based on target perceivability. *IEEE Transactions on Aerospace and Electronic Systems*, 2022, vol. 58, no. 1, p. 108–123. DOI: 10.1109/TAES.2021.3098113

[21] JIN, K., CHAI, H., SU, C., et al. Variational Bayesian adaptive filter based on variable attenuating factor (in Chinese). *Journal of Beijing University of Aeronautics and Astronautics*, 2022, vol. 49, no. 11, p. 1–16. DOI: 10.13700/j.bh.1001-5965.2021.0799

[22] LI, S., DENG, Z., FENG, X., et al. Variational Bayesian inference-based airborne radar target tracking algorithm in strong clutter (in Chinese). *Acta Electronica Sinica*, 2022, vol. 50, no. 5, p. 1089–1097. DOI: 10.12263/DZXB.20210374

[23] SARKKA, S., NUMMENMAA, A. Recursive noise adaptive Kalman filtering by variational Bayesian approximations. *IEEE Transactions on Automatic Control*, 2009, vol. 54, no. 3, p. 596–600. DOI: 10.1109/TAC.2008.2008348

About the Authors ...

Longyuan XU was born in Shandong, China. He received B.S. and M.S. degrees from HIT in 2020 and 2022. He is currently working on the Doctorate degree in Information and Communication Engineering from HIT. His research interests include the fields of data processing of HF OTH radar.

Peng TONG obtained a Ph.D. in Engineering in 2018 and currently holds a position as an Associate Researcher at the School of Electronics and Information Engineering, Harbin Institute of Technology. His primary research focuses on interference and clutter suppression in complex backgrounds in radar signal processing, as well as data processing in radar applications within environments characterized by high clutter.

Yinsheng WEI (corresponding author) was born in 1974. He received his M.S. and Ph.D. degrees in Communication and Information Systems from Harbin Institute of Technology (HIT) in 1998 and 2002, respectively. And then, he joined the Department of Electronics Engineering in HIT as a lecturer, and became a Professor in 2011. His current research interests include anti-jamming radar waveform design, radar signal processing, and radar system analysis and simulation.